



# Stabilization of furanics to cyclic ketone building blocks in the vapor phase

Taiwo Omotoso, Leidy V. Herrera, Tyler Vann, Nicholas M. Briggs, Laura A. Gomez, Lawrence Barrett, Donald Jones, Tram Pham, Bin Wang, Steven P. Crossley\*

School of Chemical, Biological and Materials Engineering, University of Oklahoma, 100 E. Boyd St. Rm T-301, Norman, OK, 73071, United States

## ARTICLE INFO

### Keywords:

Biomass  
Furfural  
Spillover  
Cyclopentanone  
Torrefaction

## ABSTRACT

Furanics are produced in high abundance from the decomposition of biomass. The thermal and chemical instability of these species leads to the formation of humins upon condensation. The ring rearrangement of furfural to form 2-cyclopentenone and cyclopentanone is known to occur in the condensed aqueous phase, but this requires operation in condensed acidic media where humin formation readily occurs. High hydrogen pressures are typically used to offset rapid polymerization reactions, limiting the yields of stable unsaturated products that result. Here we report that furfural can be selectively converted to 2-cyclopentenone and cyclopentanone in a single step over supported  $\text{TiO}_2$  catalysts with both model compounds and real biomass-derived streams in the vapor phase. Selectivity for ring rearrangement vs. C–O cleavage over  $\text{TiO}_2$  supported Ru and Pd catalysts can be tuned by manipulating the water partial pressure. The formation of these products in the absence of a condensed acidic stream also enables the tuning of reaction environments to favor the selective formation of unsaturated ketones, which could be valuable diolefin precursors. The incorporation of a  $\text{TiO}_2$  support in the catalysts tested leads to the suppression of C–C hydrogenolysis/decarbonylation and enhancement of ring rearrangement reactions. The nature of the active sites for selective C–O cleavage as well as vapor phase ring rearrangement are discussed.

## 1. Introduction

Furanic species are well known products of biomass degradation. Furanic species are produced from biomass in high abundance from biomass via both thermal and chemical routes, including hydrolysis and pyrolysis. The selective conversion of furanics to higher value products while minimizing side reactions such as the formation of humins remains a challenge. A wide range of reactions have been proposed to yield higher value products from furanics [1–4], but the ring rearrangement reaction to form cyclic ketones holds particular promise. This reaction is commonly referred to as a Piantacelli ring rearrangement when preformed in the condensed aqueous phase.

The formation of cyclopentanone (CPNO) and its derivatives from the ring rearrangement of furanic molecules such as furfural (FAL) is promising for a variety of reasons. CPNO is more stable than FAL and more amenable to long term storage and transportation than its furanic counterpart [5]. In addition, CPNO is capable of undergoing self-aldol condensation reactions to form jet fuel precursors, unlike FAL [6–8]. CPNO is a valuable specialty chemical as well, serving as an important intermediate for the production of a variety of polymers and pharmaceutical chemicals and a feedstock for jet fuel precursor production

[9–11]. The flexibility of CPNO as a high value commodity chemical as well as a fuel precursor make it an attractive target for improving biorefinery profitability as well as energy return on investment [12].

The production of the partially unsaturated precursor, 2-cyclopentenone (2CPNE), potentially holds even more value. The market for this chemical has not been studied to the same extent as CPNO due in part to the difficulty in capturing this intermediate under typical CPNO production conditions. When coupled with a highly oxophilic metal to create the unsaturated alcohol and a Lewis acid to subsequently dehydrate the alcohol, 2CPNE has the potential to be selectively converted to cyclopentadiene. Oxophilic metals that have shown high selectivities towards hydrogenating carbonyl groups in the presence of unsaturated C=C bonds, such as doped bimetallic catalysts, Pd–Cu [13] or Ni–Fe [14], or molybdenum based catalysts [15], could serve this purpose. More recent results indicating the ability of water to manipulate selectivity to favor hydrogenation of oxygen groups through the creation of a hydrogen bonded network [16–18] could also enable the formation of unsaturated alcohols. When the unsaturated alcohols are passed over a Lewis acid or a weak Bronsted acid, such as phosphorous containing zeolites [19], cyclic diolefins may result. This pathway should be the focus of follow up studies, but this could be yet another promising

\* Corresponding author.

E-mail address: [stevenccrossley@ou.edu](mailto:stevenccrossley@ou.edu) (S.P. Crossley).

<https://doi.org/10.1016/j.apcatb.2019.04.079>

Received 13 August 2018; Received in revised form 7 April 2019; Accepted 22 April 2019

Available online 23 April 2019

0926-3373/ © 2019 Published by Elsevier B.V.

benefit of carrying out this FAL conversion chemistry at elevated temperatures in the vapor phase such that these high value products can conceivably be produced. Cyclopentadiene undergoes rapid Diels Alder cycloaddition to form dicyclopentadiene, which has a market upwards of 165,000 tons/year for use in resins [20]. Dicyclopentadiene is currently produced via naphtha cracking, and renewable sources to replenish this diminished market could hold great promise.

Initial studies focusing on this reaction proposed a pathway via the rearrangement of a 2-furyl carbinol into 4-hydroxy-2-cyclopentenone (4-HCP) in an acidic aqueous environment [21]. It has been shown that the presence of water is necessary for this reaction to occur, and that the reaction rate is enhanced in an acidic environment [9,22–24]. Unfortunately, the conditions that are known to favor the ring rearrangement (acidic aqueous conditions) are also the same conditions that are known to benefit undesirable humin formation [24]. Furanic species have a well-known propensity to form humin species when stored even at room temperature in bio-oil mixtures [25–28]. The possibility to convert these furanic species in the dilute vapor phase prior to condensing to a liquid phase has the potential to significantly increase yields and improve the overall thermal stability of the resulting product. A selective surface reaction may also enable the production of 2CPNE, as excessive hydrogen pressures are not required to avoid subsequent polymerization of products in the acidic environment.

While a great deal of effort has been dedicated to the transformation of FAL and other furanics in the vapor phase [29–33], products observed are typically limited to furfuryl alcohol (FOL), 2-methylfuran (2MF), furan (FUR) and cracking products [34–38]. Here we show that  $\text{TiO}_2$  supported catalysts in the presence of water vapor at elevated temperature and atmospheric pressure can catalyze ring rearrangement reactions in the absence of a condensed phase. The introduction of water shifts the selectivity from 2MF to 2CPNE and CPNO, while also decreasing excess hydrogenolysis to form light gases. The model compound studies were found to be in good agreement with the reaction of Red Oak torrefaction feeds that contained a mixture of furfurals, acids/esters and an excess of water where both CPNO and 2MF were produced. The role of the metal/support interface as well as defects on the  $\text{TiO}_2$  support on this reaction are discussed.

## 2. Experimental

### 2.1. Catalyst preparation

Ru and Pd catalysts were synthesized using the incipient wetness impregnation method of an aqueous solution of hexaamineruthenium (III) chloride (98% Sigma Aldrich) and palladium (II) nitrate dihydrate, respectively, on the  $\text{TiO}_2$  support (Aeroxide P25, 0.25 ml/g pore volume) or  $\text{SiO}_2$  support (Hisil-210, 0.96 ml/g pore volume). The catalysts were then dried at room temperature in air for 48 h, at 120 °C for 12 h in an oven before reducing at 400 °C for 2 h in hydrogen flow. The catalysts were pelletized and sieved to yield pellet sizes from 250 to 420  $\mu\text{m}$ .

### 2.2. Catalyst characterization

Inductively coupled plasma mass spectrometry (ICP-AES) was utilized to determine Ru content of the synthesized catalysts, since Ru is known to have high mobility during reduction and can form volatile oxides upon calcination which can decrease the total amount of the metal on the catalyst [39]. Ru and Pd particle size distributions were obtained using Transmission Electron Microscopy (TEM, JEOL JEM-2100 model). Before imaging, the catalysts were pre-reduced in hydrogen flow at 400 °C for 1 h and cooled down to room temperature in nitrogen before dispersion in isopropanol and sonication to obtain a uniform suspension. A few drops of the suspension were dispersed on carbon-coated copper TEM grids. At least 200 particles were counted in order to obtain particle size distributions, which are shown in Figs. S1–S10.

### 2.3. Catalytic activity tests

Catalytic activity was tested in a quartz tube packed bed flow reactor (0.25 in OD) at atmospheric pressure and 400 °C. Catalyst particles (250–420  $\mu\text{m}$ ) were mixed with inert acid-washed glass beads (Sigma Aldrich, Part number: G1277) with a particle size range of 212–300  $\mu\text{m}$  and packed between two layers of quartz wool inside the reactor. In a typical experiment, pure distilled furfural (obtained from Sigma Aldrich; distilled and stored at –15 °C) with a feed flow rate of 0.1 ml/h was fed or co-fed with water 0.25 ml/h (18 M $\Omega$  water was obtained from an in house filtration system) or  $\text{D}_2\text{O}$  (Deuterium Oxide, 99.9% D, Sigma Aldrich, 151882). The feed was vaporized at the inlet zone of the reactor before introduction into a 30 ml/min hydrogen flow. The outlet stream of the reactor was heated to 250 °C to prevent condensation of compounds in the transfer lines and then directed through a six-port valve to allow for injection into a GC for product analysis. Product distribution was analyzed by online gas chromatography equipped with a flame ionization detector (Agilent 5890), and HP-INNOWAX column (30 m, 0.25  $\mu\text{m}$ ). Identification of products was confirmed using a Shimadzu QP-2010 GC-MS and standards were used to quantify the various products in the FID. Before introduction of the feed, the catalysts were reduced in situ at 400 °C for 1 h in 100 ml/min hydrogen flow. Mass balances for all the reactions were > 94% unless otherwise noted.

### 2.4. Oak torrefaction experiments

Experiments with real biomass vapors were conducted with Red Oak sawdust ground to 0.25–0.45 mm and dried in a vacuum oven (0.02 MPa) at 60 °C for 24 h. Sample sizes consisting of 0.7–1.0 mg red oak were packed in a quartz sample tube for use in a pyroprobe CDS analytical Model 5250 with an autosampler. The heating chamber in the pyroprobe is a quartz chamber that was heated to 270 °C for 20 min in 20 ml/min inert helium carrier gas. The vapors produced over the 20 min travel through the transfer lines where a 20 ml/min hydrogen stream is introduced. Hydrogen is introduced downstream of the torrefaction reactor to ensure that torrefaction is carried out under an inert environment. After passing through the catalyst bed, the vapors are collected in a sorbent trap maintained at –50 °C by use of liquid  $\text{N}_2$ . The trap is then desorbed at 300 °C for 3 min and the vapors passed through 1/16" Silcosteel transfer lines at 300 °C to a separate quartz reactor setup for ex-situ upgrading. An 8" quartz reactor tube placed inside a 2" ID x 6" Fibercraft Heater was connected to the pyroprobe transfer lines. 1.0 mg of Ru/ $\text{TiO}_2$  catalyst was mixed thoroughly with 200 mg acid washed borosilicate beads (Sigma Aldrich G1145) to prevent channelling. The catalyst bed was maintained halfway through the quartz reactor by use of 30 mg of quartz wool. Temperature was measured directly outside of the quartz reactor tube by use of an Omega type K thermocouple.

Analysis of the vapor product stream was carried out using an online Shimadzu QP2010 GC-MS-FID system equipped with a RTX-1701 column (60m x 0.25 mm with 0.25  $\mu\text{m}$  film thickness). The column oven heating ramp was set to hold at 4 min at 45 °C then ramp at 3 °C/min to 280 °C and hold for 20 min. A helium carrier gas was used with a total flowrate of 90 ml/min and a column flowrate of 1 ml/min. The products were identified by literature mass spectral data and quantified using FID peak area. Calibration injections of several known torrefaction products were applied to determine the molar amounts of each compound in the product stream.

The mass spectrum allowed for identification of each product using the mass fragmentation patterns and literature while yields were determined using the FID area of a peak normalized to 1 mg of biomass fed. The FID/MS split ratio was set to 10:1. A calibration was then applied to determine the  $\mu\text{g}$  of carbon/mg biomass. This was done using an effective carbon number (ECN) model which relates the FID signal to the number of carbon atoms in each molecule based on its molecular

structure, therefore accounting for the influence of various C–O bonds and other functional groups on the FID signal. Due to the large amount of compounds present in pyrolysis/torrefaction, traditional model compound injection calibrations for each species were not feasible. This model has been used extensively for the quantification of compounds found in oak pyrolysis. The model was validated with our own experimental calibrations of 42 compounds, including typical compounds of light oxygenates, sugar derivatives and phenolic categories.

## 2.5. Synthesis of nanotube supported catalysts

Carbon nanotube supported catalysts with varying distances of separation between potential active sites were prepared using an identical procedure and apparatus as described in our recently published manuscript [40]. A more detailed description of the synthesis procedure can be found in this reference. Briefly, carbon nanotube forests were grown on silicon wafers by spin coating iron, cobalt, and aluminum precursors on the surface of the wafer, followed by drying and calcination. Nanotubes were synthesized at a reaction temperature of 675 °C under flowing ethylene as the carbon source after the previously described reduction and pretreatment. Nanotube forest samples were then heated in air at 480 °C to remove amorphous carbon deposits and facilitate the removal of the forest from the silicon wafer. Palladium and titanium were deposited on the surface of the wafer by thermal evaporation in our previously described homebuilt evaporator system. In order to deposit metals on opposing ends, the sample was manipulated by using aluminum tape containing a carbon adhesive after Pd incorporation. Ti was then evaporated on the opposing end of the nanotube forest. The carbon residue was removed by soaking the sample in isopropanol to dissolve the adhesive. The sample was then calcined at 350 °C to oxidize the Ti to form TiO<sub>2</sub>, the oxidation state of which has been confirmed with both TPR and XAS in our prior publication. The Pd/CNT/TiO<sub>2</sub> catalyst contains 0.3 wt% Pd and 0.65 wt% TiO<sub>2</sub>, while the Pd/TiO<sub>2</sub>/CNT catalyst contains 0.38 wt Pd and 0.64 wt% TiO<sub>2</sub>. Weight loadings of Pd and Ti were determined via a calibrated quartz crystal microbalance.

## 2.6. Density functional theory calculations

The DFT calculations were performed using the VASP package [41]. The PBE (Perdew-Burke-Ernzerhof) exchange-correlation potential [42] was used, and the electron-core interactions were treated in the projector augmented wave (PAW) method [43,44]. The van der Waals interaction was included using the so-called DFT-D3 semi-empirical method [45,46]. The calculations have been performed using a (2 × 5) rutile TiO<sub>2</sub> (110) surface, which consists of 6 O–Ti–O layers with overall 120 Ti and 240 O atoms. The top three O–Ti–O layers were free to relax while the bottom three layers were fixed at the optimized bulk positions. The lattice constants of the DFT-optimized TiO<sub>2</sub> bulk structure were  $a = b = 4.596$  and  $c = 2.950$  Å. A Ru cluster consisting of 10 atoms was positioned on top of the TiO<sub>2</sub> surface, and the vacuum layer was set to more than 14 Å between adjacent supercells. The atoms were relaxed until the atomic forces were smaller than 0.02 eV Å<sup>-1</sup>, using a single  $\Gamma$  point of the Brillouin zone with a kinetic cutoff energy of 400 eV. A rotationally invariant DFT + U approach was applied [47]; the effective parameters, U and J, of Ti atoms to include the Hubbard on-site Coulomb repulsion were chosen as 2.5 and 0 eV, respectively [48]. When comparing molecular adsorption on a clean Ru surface, a model with a four-layer (4 × 4) Ru (0001) plane was used, and the lattice constant of Ru bulk was taken from a previous report [49].

## 3. Results and discussion

### 3.1. Reaction of pure furfural over Ru/TiO<sub>2</sub>

Product distributions for FAL conversion over Ru/TiO<sub>2</sub> in the vapor

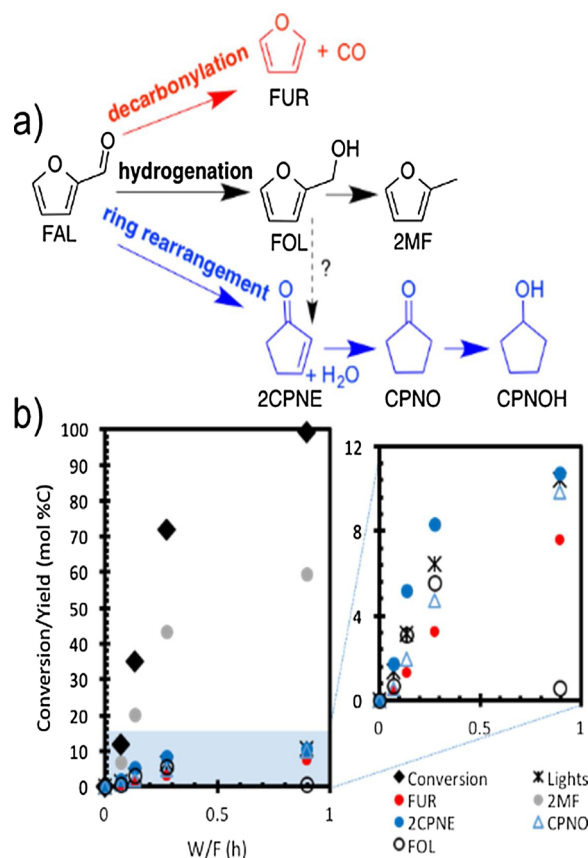


Fig. 1. a) schematic of FAL conversion to various products. b) FAL conversion and product yield with W/F over 4.4% Ru/TiO<sub>2</sub> at 400 °C. 1 atm, TOS: 30 min. Carbon balance ~95% all reactions.

phase are shown in Fig. 1. The most abundant product, 2MF (yield = 59.7% at 0.9 h), is produced from the hydrogenolysis of the C–O bond of FOL. Others have shown that the combination of metals with oxophilic sites can facilitate the selective cleavage of this bond [50]. While it is known that this selective C–O cleavage can occur over metal surfaces [2,51–53], interfacial sites formed as a result of the interaction between Ru and the reducible oxide TiO<sub>2</sub> can play an important role in the formation of 2MF from FOL as seen by their proposed importance in reactions such as Fischer-Tropsch synthesis [54], phenol hydrodeoxygenation [55], and alkane hydrogenolysis [56].

The unanticipated reaction products observed under these conditions are 2CPNE and CPNO. Both of these products appear to increase at higher W/F values (W/F, defined as grams of catalyst/grams of FAL fed per hour), while FOL yields pass through a maximum (yield = 5.5% at 0.3 h). This result implies that FOL is subsequently converted to 2MF or possibly 2CPNE/CPNO at higher W/F values. FOL can be formed from direct hydrogenation of the carbonyl C–O bond of FAL on the Ru metal. This reaction has been shown to occur over various metal catalysts such as Pt, Pd, Cu and Ni in liquid and gas phase [2,22,51–53]. To obtain FOL, the O atom in the carbonyl group of FAL can adsorb on top of the Ru surface in an  $\eta^1$  configuration as has been reported over Cu catalysts [53,57].

FAL can also adsorb on metal surfaces with both C and O atoms bound to the surface in an  $\eta^2$  mode [53,58,59]. At higher temperatures, the metal oxygen bond of the  $\eta^2$  intermediate may break to form a surface acyl, which is a precursor to decarbonylation to produce FUR. Catalysts with oxophilic sites have been shown to stabilize the metal oxygen bond more strongly and hinder the formation of surface acyl species [2], leading to decreased selectivity to decarbonylation products. This may be occurring at the Ru/TiO<sub>2</sub> interface in this case.

The unexpected formation of 2CPNE and the subsequent

hydrogenation of the olefin to form CPNO represent the most interesting products observed here. From Fig. 1, the yield of these products increase steadily as the W/F increases. The yield of the ring rearrangement products increased at higher W/F values, with the H<sub>2</sub>O partial pressure also increasing along the reactor bed due to the in-situ water generated from 2MF production.

### 3.2. Role of water for furfural conversion to cyclopentanone

The importance of water for the ring rearrangement reaction to occur in the liquid phase has been discussed extensively in literature [22–24], but this reaction has not been investigated in the vapor phase. It should be noted that even though water was not introduced as a reactant in the results presented above, the CPNO/2CPNE products were still observed. Water can be produced in small quantities in-situ via the hydrogenolysis of FOL to form 2MF as discussed earlier.

The ring rearrangement reaction in the condensed aqueous phase has been the subject of a variety of studies in recent years. An important point that must be considered is the role of the catalyst surface on this reaction in acidic aqueous solutions. While the mechanism of this reaction is different in the condensed phase from, it is important to distinguish the different mechanisms that have been proposed to explain this reaction in the liquid phase. Initial proposals for ring rearrangement chemistry from FAL were thought to occur solely through an aqueous acid catalyzed reaction. The role of the metal was simply to hydrogenate the FAL to form FOL and then to subsequently hydrogenate formed products to ultimately produce cyclopentanol. Evidence in support of this comes from the fact that simply by placing FOL in an acidic aqueous environment at elevated temperatures, ring rearrangement to form 4-HCP (Fig. 2a) is observed. An unfortunate consequence of acid chemistry alone is the poor carbon balances that result due to formation polymer side products [60]. The addition of metals and bi-metallic catalysts to convert intermediates in situ have led some to propose alternative mechanisms. Due to the absence of the observation of 4-HCP, Hronec et al. have proposed that the acidic aqueous solution first facilitates dehydration of FOL, followed by ring opening with intermediates stabilized on a metal surface as shown in Fig. 2b [60]. Hronec et al. proposed that the metal hydrogenates these surface species to prevent further polymerization and increase yields to ring rearrangement products when compared to those observed in the absence of a metal catalyst.

To determine whether gas phase water is involved in this rearrangement, furfural was co-fed with excess water in a molar ratio of 12:1 at different conversions, with the results presented in Fig. 3a. With the introduction of water, the sum of the CPNO/2CPNE products (yield = 16%) is similar to the yield of 2MF (yield = 17%). Comparing this with the values obtained without water in the feed, CPNO/2CPNE (yield = 7%), 2MF (yield = 20%) an enhancement in the rate of the ring rearrangement reaction is clearly observed when water is introduced to the system. The role of the support on this reaction will be discussed in the following section.

### 3.3. Active sites responsible for conversion over Ru/TiO<sub>2</sub> and Pd/TiO<sub>2</sub>

TiO<sub>2</sub> supported catalysts have been shown to exhibit several possible types of active sites for the selective activation of C–O bonds, ranging from the creation of new sites at the metal support perimeter to the presence of defects, or promoter effects on the support [39,61]. For the conversion of phenolic oxygenates, enhanced rates of C–O cleavage have been reported when the reducible oxide TiO<sub>2</sub> was introduced as a support, which was attributed to the synergy between Ru and TiO<sub>2</sub> [61]. Further studies showed that defect sites on the TiO<sub>2</sub> support are the active sites for the initial transalkylation step of guaiacol conversion [42], while the subsequent C–O bond cleavage required for the conversion of cresol to toluene occurs as a result of active sites around the perimeter of the metal particle [62].

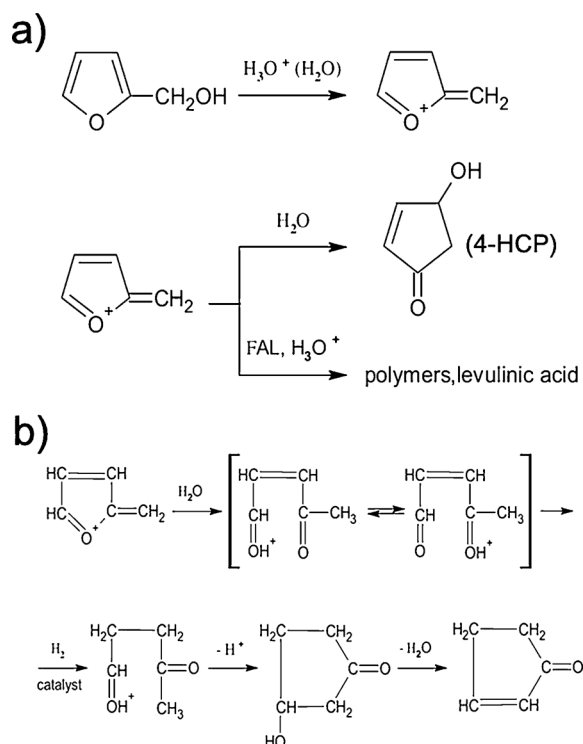
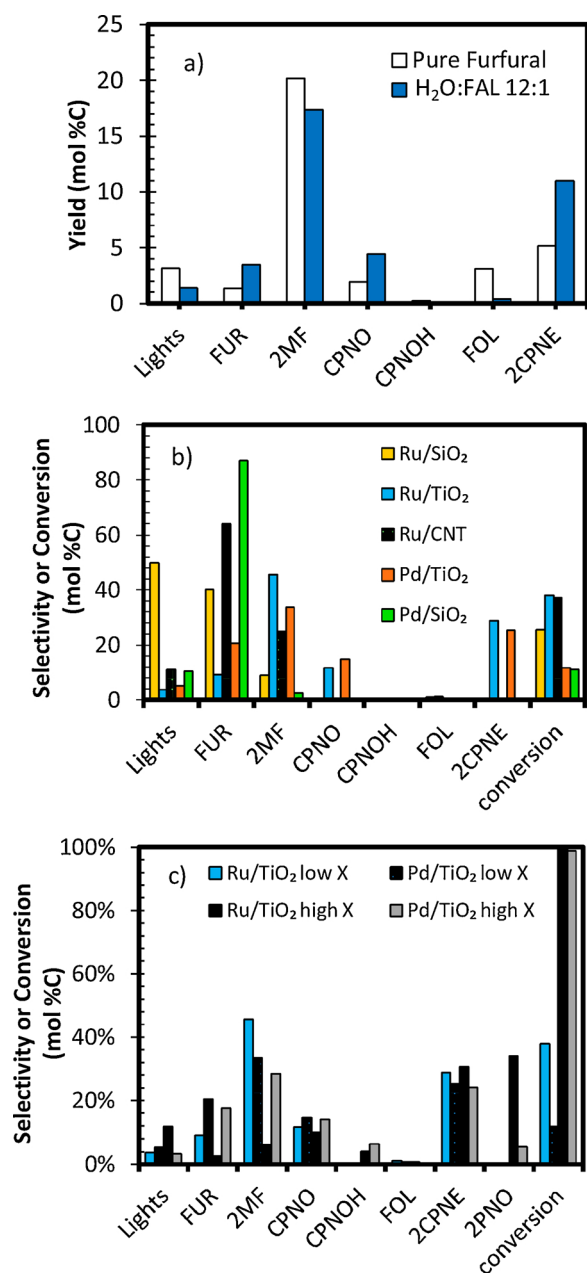


Fig. 2. Adaptations from literature reports to explain ring rearrangement chemistry in the condensed aqueous phase. a) Schematic of FOL conversion in aqueous media to form charged dehydrated species that undergo rearrangement to form 4-HCP or polymerization. b) Proposed surface stabilized intermediates in the condensed aqueous phase stabilized on a metal surface leading to ring rearrangement products. Adapted from [60].

To investigate the importance of active sites on the support for this rearrangement, pure Ru catalysts supported on SiO<sub>2</sub> and carbon nanotubes (CNT) and a bare TiO<sub>2</sub> catalyst with no metal loading were compared with Ru/TiO<sub>2</sub>. The results obtained from feeding a water/FAL (12:1 M ratio) mixture over these catalysts are presented in Table 1. Ru can facilitate the splitting of water leading to decoration of the Ru metal surface with OH groups, which could potentially play a role in this reaction [63–65] although as we will show later this is not the cause of the ring rearrangement activity observed under these conditions. We shall proceed by discussing the difference in product selectivity observed over the pure Ru catalysts on inert supports (Ru/SiO<sub>2</sub> and Ru/CNT) and Ru/TiO<sub>2</sub> as shown in Fig. 3b (with product yields reported in Fig. S16). The following are evident: 1) CPNO and 2CPNE are only observed over Ru catalysts supported on TiO<sub>2</sub>. 2) An enhancement in FAL conversion to 2MF, which is also a valuable product, is observed when compared to Ru supported on the other tested supports. 3) Decarbonylation and C–C hydrogenolysis rates are suppressed on Ru/TiO<sub>2</sub> when compared to other supported Ru catalysts.

With increasing conversion there is shift in selectivity to favor ring rearrangement products over Ru/TiO<sub>2</sub> with yields of ~45% (2CPNE + CPNO + CPNOH) becoming dominant products of the reaction at higher conversions. At the high conversion (> 98%), other reactions such as ring opening to form 2-pentanone (2PNO) likely from 2MF and C4 (Butanal and butanol) from FUR are observed as shown in Fig. 3c. Low yields from the hydrogenation of the ketone to form cyclopentanol (CPNOH) are also detected at higher conversion levels. Similar trends are observed with Pd/TiO<sub>2</sub> at high conversions, with lower selectivities to ring opening products, but higher selectivities to decarbonylation products and methylfuran. Note that the Ru particle size (Table S1) of the TiO<sub>2</sub> supported catalyst lies within the range of particle sizes observed over carbon and silica supports, so particle size





**Fig. 3.** a) Product distribution for pure furfural and furfural co-fed with water. 4.4% Ru/TiO<sub>2</sub> at 400 °C, 1 atm, and 30 min time on stream. Conversion = 36 ± 2%. Carbon balance > 94% for all reactions. b) Product selectivity and conversion for water/furfural (12:1 M ratio) feed mixture over Ru/SiO<sub>2</sub>, Ru/CNT and Ru/TiO<sub>2</sub> catalysts W/F = 0.13 h (Ru/SiO<sub>2</sub>, Ru/TiO<sub>2</sub>, Pd/SiO<sub>2</sub>, and Pd/TiO<sub>2</sub>) and 0.39 h (Ru/CNT) T = 400 °C, P = 1 atm, TOS = 30 min. c) Comparison of data reported in b) over TiO<sub>2</sub> supported catalysts at low and high (> 98%) conversions obtained at higher W/F values.

and coordination number cannot explain the behavior observed here.

Water may promote longer catalyst lifetimes as well. Fig. S11 shows conversion vs. time on stream for furfural conversion in the presence and absence of water. After 3 h on stream, 71% of the activity is lost (when compared to the rate obtained after extrapolation to 0 time on stream) for furfural conversion alone. In the presence of water, however, there is a 56% reduction in activity over that same time period. This implies that water may be either cleaning the surface or minimizing readsorption of coke forming precursors.

This enhancement to form desired products (CPNO/2CPNE and 2MF) as a result of the introduction of TiO<sub>2</sub> as a support could be due to

either sites located around the perimeter of the metal particle, or exposed cations on the TiO<sub>2</sub> surface. To understand this further, the same reaction was conducted over pure TiO<sub>2</sub> without the Ru metal. As seen in Table 1, when passing FAL and water over TiO<sub>2</sub> alone, small amounts of 2CPNE/CPNO are observed, but due to the lack of a metal that promotes the dissociation of hydrogen, nearly an order of magnitude higher TiO<sub>2</sub> catalyst amount is necessary to achieve the same level of conversion as with metal supported on TiO<sub>2</sub>. If sites at the metal/support interface are directly involved in the ring rearrangement reaction, one would anticipate significant shifts in reaction rate with the carbon-metal and carbon-oxygen bond strength. To further probe the role of the metal, the FAL reactions with water were carried out over Pd supported on TiO<sub>2</sub>, with Pd forming much weaker bonds with both carbon and oxygen than Ru [66]. The role of Pd at opening the furanic ring at interfacial sites is anticipated to be very different. Considering spillover to the TiO<sub>2</sub> support to create defects, however, Rekoske and Barteau reported indistinguishable isothermal TiO<sub>2</sub> reduction profiles when the two metals were added in similar quantities to a TiO<sub>2</sub> support [67]. This implies that the different behaviour between the two catalysts likely involves the direct interaction of the metal with the furanic species, as opposed to a simple shift in the number of defects on the TiO<sub>2</sub> support at steady state. In Fig. 3b the production of CPNO/2CPNE over Pd/TiO<sub>2</sub> is clearly lower than observed for Ru/TiO<sub>2</sub>, but it is still present.

Table 1 shows the rate of formation of various products normalized per metal exposed (Ru or Pd), per TiO<sub>2</sub> surface area, and per perimeter area surrounding the nanoparticles for TiO<sub>2</sub> supported catalysts. Ru/TiO<sub>2</sub> is the most effective catalyst tested for forming ring rearrangement products. When compared with the TiO<sub>2</sub> support alone, the reaction rate is enhanced by approximately 40x when Ru is incorporated, implying that the reaction can occur over defects alone, but the rate of this reaction is negligible when compared to rate in the presence of a metal.

In the condensed aqueous phase ring rearrangement reaction, it is generally accepted that the role of the metal is to hydrogenate the FAL to form FOL, with subsequent ring rearrangement reactions in the acidic aqueous phase to form CPNO precursors such as unsaturated hydroxycyclopentanones or ring opened intermediates [6,24]. Hronec et al. proposed that the metal could play the additional role of conversion of these active intermediates that are produced in the acidic aqueous phase to limit side products produced from polymerization/humin formation [60]. Rates of 2CPNE/CPNO production when feeding intermediate products (FOL and 2MF) can be used to determine the kinetic relevance of pathways involving these intermediates. As shown in Table 2 when feeding 2MF no CPNO/2CPNE was observed, which illustrates that it is not a relevant intermediate for the reaction. Surprisingly, when feeding FOL, the yield of CPNO/2CPNE is lower than was observed when FAL was fed over Pd/TiO<sub>2</sub>. This indicates that FAL itself can undergo ring rearrangement prior to desorbing from the surface, and the role of the metal is not to simply supply hydrogen to create defects and yield alcohol intermediates that react on the TiO<sub>2</sub> support. These results suggest that the active site for this reaction lies at the interface of the metal and the TiO<sub>2</sub> support. In order to gain further proof of the interface as the active site, the reaction co-feeding FAL and water was tested over a physical mixture composed by Ru/SiO<sub>2</sub> and TiO<sub>2</sub> (Table 1). No significant yields to ring rearrangement products were observed at the tested W/F when the physical mixture was used. It should be noted that while some yield to these products is expected over the TiO<sub>2</sub> used in the physical mixture, the rate is sufficiently low to not observe significant quantities under the conditions tested.

In order to further clarify the role of the support, we carried out reactions using a technique we have recently demonstrated as capable of distinguishing sites at the metal-support interface from traditional promoter effects. This is accomplished by using carbon nanotube supports serving as a bridge to allow the Pd metal to spillover hydrogen to partially reduce the surface of the TiO<sub>2</sub> while not being in physical contact. The experimental procedure for preparation, as well as detailed

**Table 1**

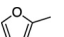
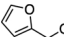
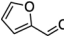
Rate of products normalized per exposed metal, support, or metal-support perimeter.

Catalyst	Conversion (%)	Rate product/exposed metal (mol/m <sup>2</sup> h)			Rate /Per TiO <sub>2</sub> (mol/m <sup>2</sup> h)	Rate/Per Perimeter (mol/m h)	Carbon Balance (%)
		FUR	LIGHTS	2CPNE + CPNO			
Ru/SiO <sub>2</sub>	25	1.23*10 <sup>-03</sup>	2.53*10 <sup>-03</sup>	–	–	–	95
Ru/CNT	37	5.55*10 <sup>-03</sup>	9.51*10 <sup>-04</sup>	–	–	–	94
Ru/TiO <sub>2</sub>	38	4.42*10 <sup>-04</sup>	1.78*10 <sup>-04</sup>	1.95*10 <sup>-03</sup>	1.96*10 <sup>-04</sup>	3.52*10 <sup>-12</sup>	95
Pd/SiO <sub>2</sub>	11	4.98*10 <sup>-03</sup>	6.02*10 <sup>-04</sup>	–	–	–	96
Pd/TiO <sub>2</sub>	12	6.22*10 <sup>-04</sup>	1.57*10 <sup>-04</sup>	1.21*10 <sup>-03</sup>	5.96*10 <sup>-05</sup>	1.03*10 <sup>-12</sup>	96
Ru/SiO <sub>2</sub> -TiO <sub>2</sub> (Physical mix)	16	1.81*10 <sup>-03</sup>	2.98*10 <sup>-03</sup>	–	–	–	94
TiO <sub>2</sub>	10	–	–	–	5.14*10 <sup>-06</sup>	–	94

\*All reactions conducted at a water/FAL (12:1 M ratio) feed mixture. W/F = 0.13 h (Pd/SiO<sub>2</sub> and Pd/TiO<sub>2</sub>), Conversion = 11.12% (1%Pd/SiO<sub>2</sub>) and 12.05%(1% Pd/TiO<sub>2</sub>), W/F = 1.85 h (TiO<sub>2</sub>) and 0.13 h (Ru/SiO<sub>2</sub> and Ru/TiO<sub>2</sub>) and 0.39 h(Ru/CNT) Conversion = 10% (TiO<sub>2</sub>); 25%(5.3% Ru/SiO<sub>2</sub>); 38% (4.4% Ru/TiO<sub>2</sub>) and 37% (1% Ru/CNT) T = 400 °C, P = 1 atm, TOS = 30 min.

**Table 2**

Yield of products for reactions feeding different possible intermediates for the ring rearrangement.

Catalyst	Entry <sup>a</sup>	Yield Products (%)					Carbon Balance (%)
		2CPNE	CPNO	2MF	Lights	FUR	
Pd/TiO <sub>2</sub>		–	–	–	0.59	–	93
		2.42	0.12	7.72	0.95	–	89
		2.96	1.7	3.94	0.61	2.42	96

<sup>a</sup> Reaction conditions: water/2MF: 12:1 (W/F = 0.13 h (Pd/TiO<sub>2</sub>, Conversion: 9.15%), water/FOL: 12:1 (W/F = 0.13 h Pd/TiO<sub>2</sub>, Conversion: 21.8%),water/FAL: 12:1 (W/F = 0.13 h Pd/TiO<sub>2</sub>, Conversion: 13.05%), T = 400 °C, P = 1 atm, TOS = 30 min.

characterization of these materials to confirm their separation before and after high temperature reduction and their ability to spill over hydrogen, is outlined in our recently published manuscript [40] and discussed briefly in the experimental section.

By separating the Pd and the TiO<sub>2</sub> support on opposing ends of the carbon nanotube forest, Ti<sup>3+</sup> sites are created through hydrogen spillover from the Pd to the TiO<sub>2</sub> on the opposing end of the nanotube. In our prior work where furfural was converted on these catalysts under identical conditions in the absence of co-fed water, we showed that reduction of oxides on opposing ends of the nanotube was possible through a combination of TPR and XAS experiments. We also used acetic acid ketonization as an in-situ probe of the steady state population of Ti<sup>3+</sup> sites while furfural was converted at 400 °C under atmospheric pressure hydrogen (conditions identical to those reported here in the absence of co-fed water). These experiments revealed that the rate of hydrogen spillover is sufficient to maintain a stable population of defects on the TiO<sub>2</sub> surface under these reaction conditions [40].

Results indicate that both methylfuran production as well as ring rearrangement products are produced at the metal-support interface as shown in Fig. 4. No CPNO or 2CPNE are observed when the Pd and TiO<sub>2</sub> are not in physical contact. This result supports the prior argument that FOL is not an intermediate that is equilibrated with the vapor phase, and this ring rearrangement chemistry occurs at the metal-support interface. The role of the interface for the enhanced selectivity to form 2MF as well as CPNO is intriguing, as we anticipate that these two transformations will occur through very different binding configurations. Methylfuran production at the metal support interface likely results from the furan ring interacting with the edge of the metal particle, with the oxygen interacts with a defect on the support similar to the case of cresol deoxygenation [63]. Ring rearrangement, on the other hand, requires the interaction of the furanic ring with the support as well as a water molecule, with the oxygen likely binding to the edge of

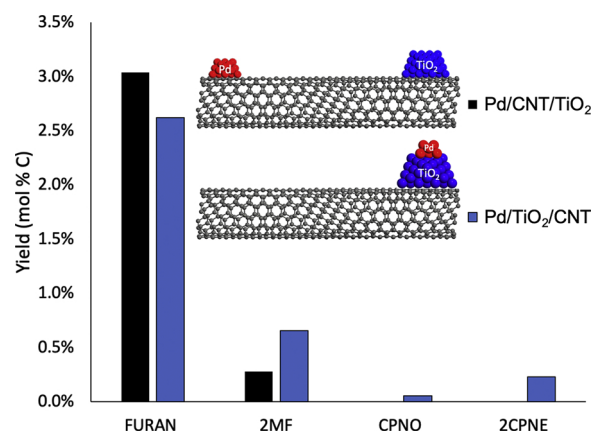


**Fig. 4.** FAL conversion over Pd and TiO<sub>2</sub> catalysts supported on CNTs at controlled distances of separation along the nanotube surface. The Pd/CNT/TiO<sub>2</sub> catalyst contains 0.3 wt% Pd and 0.65 wt% TiO<sub>2</sub>. The Pd/TiO<sub>2</sub>/CNT catalyst contains 0.38 wt Pd and 0.64 wt% TiO<sub>2</sub>. T = 400 °C, P = 1 atm, under flowing H<sub>2</sub>, 30 min time on stream (TOS). 5 mg of catalyst was used in both cases. Water was co-fed at a molar ratio of 12:1 with respect to FAL.

the metal particle. We anticipate that these two binding modes may be influenced by surface coverage and could be in competition with one another under reaction conditions.

The presence of water accelerates this reaction, even under vapor phase conditions. Further evidence of this is provided in Fig. 5. Replacing H<sub>2</sub>O with D<sub>2</sub>O reveals a significant kinetic isotope effect associated with the rate of ring rearrangement products. This suggests that the activation of the adsorbed furan ring by water is the kinetically relevant step. For comparison, decarbonylation to form methylfuran is shown to have no associated kinetic isotope effect. Differences in measured rates for the formation of all other observable products upon comparison of H<sub>2</sub>O and D<sub>2</sub>O, for example methylfuran and light products, were within the experimental uncertainty of the measurement, as shown in Fig. S12. This suggests that the deuterium present in D<sub>2</sub>O has not fully equilibrated with H<sub>2</sub>, as other reactions that involve H addition in the kinetically relevant transition state do not exhibit a primary kinetic isotope effect. A more detailed follow up study should be carried out in the future to investigate the primary and secondary kinetic isotope effects for ring rearrangement and methylfuran production while also considering the equilibrium isotope effects of prior steps, but this result does support the direct involvement of water in the kinetically relevant step.

In order to investigate the nature of interaction of FAL with sites at the metal-support interface, we explored the adsorption of FAL at the Ru/TiO<sub>2</sub> interface in comparison with a clean Ru(0001) surface using density functional theory. The most stable structures are shown in

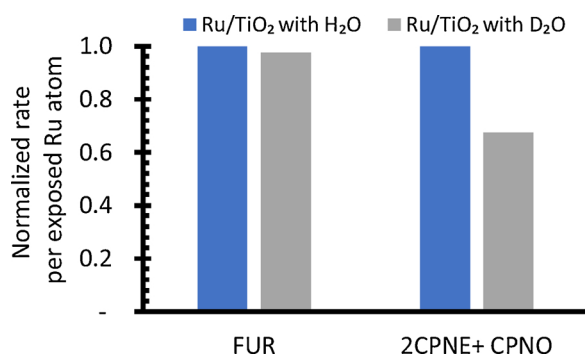


Fig. 5. Comparison of normalized rates per exposed metal atom in the presence of a 12:1 ratio of H<sub>2</sub>O or D<sub>2</sub>O to FAL. 4.4% Ru/TiO<sub>2</sub> at 400 °C, 1 atm, and 30 min time on stream. FAL conversion = 19% in the case of H<sub>2</sub>O co-feed.

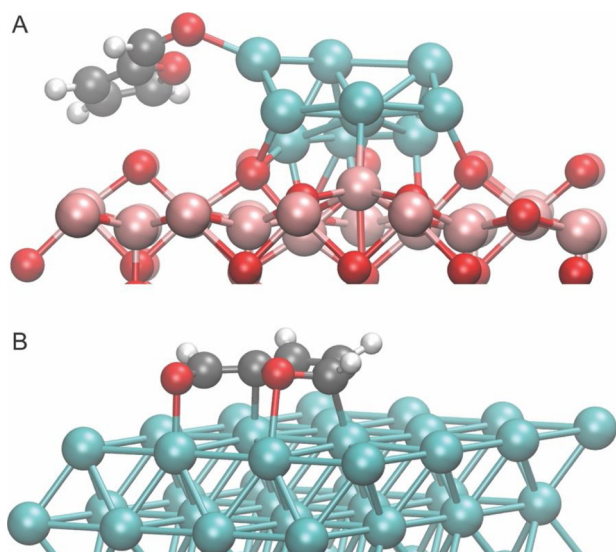


Fig. 6. DFT-optimized structures of adsorbed FAL at the Ru/TiO<sub>2</sub> interface (A) and on the Ru(0001) surface. The Ru, Ti, O, C, and H atoms are colored cyan, pink, red, gray, and white, respectively (For interpretation of the references to color in this figure legend, the reader is referred to the web version of this article).

Fig. 6. At the Ru/TiO<sub>2</sub> interface, FAL forms a  $\sigma$  bond with a low-coordinated Ru edge atom with a strong adsorption energy of  $-2.3$  eV. This interaction near the edge of the metal nanoparticle results in the furanic ring lying above the TiO<sub>2</sub> surface, where water may adsorb and assist with the ring opening and rearrangement reactions. The adsorption energy is higher on the clean Ru(0001) surface with a value of  $-2.7$  eV. The interfacial interaction is driven by the d electrons in Ru and the  $\pi$  electrons in the FAL molecule. However, it should be noted that the pair-wise semi-empirical methods, such as DFT-D3, to include van der Waals interaction may likely overestimate the molecular binding particularly on the metal surface [69]. If the van der Waals interaction is excluded, the adsorption energy of FAL at the Ru/TiO<sub>2</sub> interface and on the clean Ru(0001) are the same, both around  $-1.7$  eV. This result suggests that FAL may adsorb both at the Ru/TiO<sub>2</sub> interface and on the Ru surface. For comparison, we also calculated adsorption energy of furfuryl alcohol adsorption at the Ru/TiO<sub>2</sub> interface, and the adsorption is 0.3 eV weaker than FAL at the interface.

These results can help to explain why ring rearrangement rates and selectivities are greater when FAL is fed to the system as opposed to when FOL is fed to the system. FAL binds strongly to sites near the interface, both modifying the nature of the C–O bond while allowing a strong interaction of this surface intermediate with the TiO<sub>2</sub> surface. Because we know that water is directly involved in this reaction, there

are two general options that should be explored in more detail in a future study. These options are a) the furan ring of the surface bound intermediate interacts with an exposed Ti cation directly, making the surface intermediate amenable to attack from vapor-phase water to facilitate ring opening an rearrangement or b) water interacts with the surface of the TiO<sub>2</sub> support to facilitate the protonation of the furanic ring and subsequent ring opening. One possible explanation in support of the latter option is the enhanced protonation ability of a water molecule that has adsorbed in an oxygen vacancy site near the surface of the metal particle. We have discussed the potential of these activated water molecules as responsible for deoxygenation of cresol at the Ru–TiO<sub>2</sub> interface in a prior study [63]. These possibilities should be interrogated further by quantifying reaction orders and water adsorption enthalpy in a follow up study.

### 3.4. Oak torrefaction experiments

While the results obtained with model compounds are promising, it is important to verify that this reaction can proceed in the presence of real biomass thermal decomposition streams, which contain species such as carboxylic acids. Other species present from the thermal decomposition of biomass may strongly inhibit this reaction due to site competition. For example, we have recently illustrated that phenolic species that result from the thermal decomposition of lignin strongly adsorb to these interfacial active sites [63]. This could diminish the ability of FAL to compete for the same sites in real biomass streams. Carboxylic acids, such as the abundant acetic acid, are also known to strongly adsorb and convert over TiO<sub>2</sub> supports [70].

While streams resulting from the thermal degradation of biomass are inherently complex, these streams can significantly be simplified by conducting a staged thermal degradation. By conducting a longer low temperature torrefaction step, a stream consisting primarily of sugar derived furanic species and light oxygenates such as acetic acid is produced. The resulting solid can be subjected to subsequent thermal conversion at elevated temperature to evolve lignin derived species. The net result is a separation of phenolic compounds from a stream that consists of predominantly furanic and carboxylic acid species, allowing for more selective catalytic upgrading approaches [71]. This approach results in significant enhancements in potential yields to fuel range products when compared to single stage pyrolysis coupled with catalytic upgrading [72], as well as decreased CO<sub>2</sub> emissions for a given amount of transportation fuel produced and net increases to the energy return on investment [73].

The potential for this reaction to occur with real torrefaction vapors is illustrated in Fig. 7 by passing torrefaction vapors over a Ru/TiO<sub>2</sub> catalyst maintained at 400 °C. Results are reported after direct injection of products from the vapor phase to an online analysis system as opposed to analysis after subsequent condensation to avoid unnecessary complications due to undesired polymerization reactions that occur upon storage of bio-oil product mixtures. FAL is the second most abundant organic species present in this mixture. The composition of this stream can be found in Fig. S13. The full upgrading results over Ru/TiO<sub>2</sub> for the first biomass pulse can be found in Fig. S14. As expected, the acids and esters underwent ketonization reactions under these conditions. High levels of ketonization were observed to yield acetone and butanone from acetic acid and other C<sub>2</sub> and C<sub>3</sub> carboxylic acids and esters.

Fig. 7 illustrates that the FAL species present in the torrefaction stream reacted to produce 2CPNE/CPNO and 2MF with a selectivity to ring rearrangement products exceeding that observed in the model compound studies. FAL conversion levels of 94% were observed in the initial biomass pulse. Selectivities are reported as moles of product divided by the sum of converted FAL and the precursor to FAL, 4,5,6-trihydroxy-2H-pyran-2-one, which accounts for approximately 20% of the carbon present in these two compounds. We hypothesize that this pyranone present in the feed can form FAL via dehydration over the



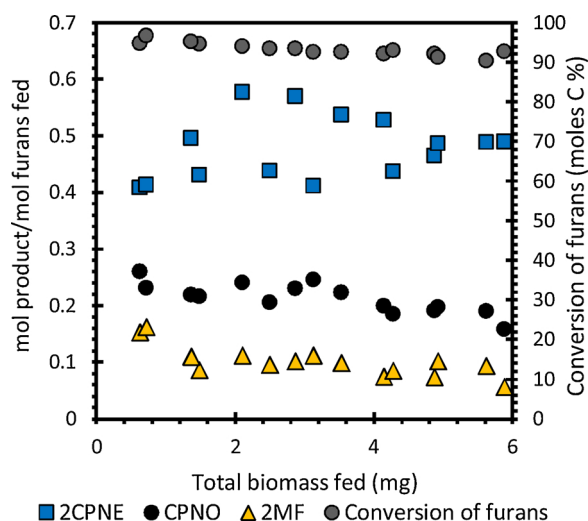


Fig. 7. Yield of products divided by the moles of FAL and pyranone fed to the reactor in a given pulse of biomass decomposition products as a function of biomass fed. Biomass torrefaction vapors were passed across a Ru/TiO<sub>2</sub> catalyst at 400 °C.

TiO<sub>2</sub> surface. It should be noted that the moles of ring rearrangement products greatly exceed the moles of pyran in the feed stream, so the predominant pathway to their formation is through the conversion of FAL. It is important to note that molar ratios of water/FAL level are even higher with this feed than with model compound studies, which may explain the high selectivity to ring rearrangement products.

The results shown in Fig. 7 correspond to a 98 ± 9% carbon balance around FAL (and pyran) derived products across the 7 pulses tested as shown in Table S2. The ratio of selectivity to ring rearrangement products (71%) when compared to 2MF (16%) is higher with real torrefaction streams, as shown in Fig. 7, when compared with the model compound studies. This selectivity to ring rearrangement products remains high with sequential biomass pulses, with yields normalized to the amount of biomass injected in each pulse. As can be seen in Fig. 7, the conversion of FAL remains high, consistently yielding 2CPNE, CPNO and 2MF as the most abundant products. It was also observed that other reactions forming ketones, such as acetone, from carboxylic acids readily occur over this catalyst in parallel (Fig. S15). The active sites required for decarboxylative ketonization appear to deactivate with time, while FAL conversion remains consistently high across the range of exposure to biomass vapors tested here.

A more detailed follow up kinetic study should be conducted to discriminate selectivity for methylfuran vs. ring rearrangement products at varying coverage, as both may occur at the metal/support interfacial sites. The role of water may also play an important role on both of these reactions, as we have recently demonstrated that C–O cleavage reactions to form toluene from cresol at perimeter sites are accelerated by the presence of water [62] at metal/support interfacial sites.

#### 4. Conclusions

Here we reveal the conditions required to selectively convert furfural to unsaturated cyclic ketones in the absence of a condensed aqueous phase. Conversion of furfural in the vapor phase at 400 °C results in a number of reactions including hydrogenation, decarbonylation, and hydrogenolysis to form products such as furfuryl alcohol, furan and 2-methylfuran. In the absence of co-fed water, minor selectivity to the carbon efficient reaction of furfural to cyclopentanone and 2-cyclopentenone was also observed. The selectivity for these reactions significantly increased as water vapor was introduced, resulting in shifts in product selectivity from 2-methylfuran to cyclopentanone and 2-cyclopentenone. The support plays an important role in

determining the product distribution as pure Ru catalysts produced mainly light gases and furan under these conditions when compared with Ru/TiO<sub>2</sub>. Experiments feeding various intermediates indicate that the vapor phase reaction does not proceed through an alcohol intermediate that desorbs from the catalyst surface. Experiments over Pd supported catalysts imply that carbon-metal and oxygen-metal bond strength at the metal/support interface likely play an important role on this reaction. Using Red Oak as a biomass source, the reaction was also observed with real torrefaction feeds in a pulse reactor. With the biomass feeds the selectivity to ring rearrangement products was enhanced beyond the levels observed with the model compound studies, illustrating the potential of this reaction to occur with furfural present in real biomass streams.

#### Acknowledgements

We acknowledge financial support from the National Science Foundation, Grant CAREER1653935, for the model compound studies and catalyst characterization presented in this work. Decomposition and conversion of red oak biomass feedstocks were supported by the U.S. Department of Energy (DOE) under grant DEEE0006287 of the Bioenergy Technologies Office CHASE (Carbon, Hydrogen, and Separations Efficiencies) program. The computational research used the supercomputer resources of the National Energy Research Scientific Computing Center (NERSC).

#### References

- [1] C.L. Williams, C.-C. Chang, P. Do, N. Nikbin, S. Caratzoulas, D.G. Vlachos, R.F. Lobo, W. Fan, P.J. Dauenhauer, Cycloaddition of biomass-derived furans for catalytic production of renewable p-xylene, *ACS Catal.* 2 (2012) 935–939.
- [2] S. Crossley, J. Faria, M. Shen, D.E. Resasco, Solid nanoparticles that stabilize biofuel upgrade reactions at the water/oil interface, *Science* 327 (2010) 68–72.
- [3] A. Gumidyala, B. Wang, S. Crossley, Direct carbon-carbon coupling of furanics with acetic acid over Brønsted zeolites, *Sci. Adv.* 2 (2016) e1601072.
- [4] G.W. Huber, J.N. Chheda, C.J. Barrett, J.A. Dumesic, Production of liquid alkanes by aqueous-phase processing of biomass-derived carbohydrates, *Science* 308 (2005) 1446–1450.
- [5] Y. Yang, Z. Du, Y. Huang, F. Lu, F. Wang, J. Gao, J. Xu, Conversion of furfural into cyclopentanone over Ni-Cu bimetallic catalysts, *Green Chem.* 15 (2013) 1932–1940.
- [6] T.V. Bui, S. Crossley, D.E. Resasco, C-C coupling for biomass-derived furanics upgrading to chemicals and fuels, *Chemicals and Fuels From Bio-based Building Blocks*, (2016), pp. 431–494.
- [7] M. Hronec, K. Fulajtárova, T. Liptaj, M. Štolcová, N. Prónayová, T. Soták, Cyclopentanone: a raw material for production of C<sub>15</sub> and C<sub>17</sub> fuel precursors, *Biomass Bioenergy* 63 (2014) 291–299.
- [8] T. Kawabata, M. Kato, T. Mizugaki, K. Ebitani, K. Kaneda, Monomeric metal aqua complexes in the interlayer space of montmorillonites as strong Lewis acid catalysts for heterogeneous carbon-carbon bond-forming reactions, *Chem. Eur. J.* 11 (2005) 288–297.
- [9] D.T. Ngo, T. Sooknoi, D.E. Resasco, Improving stability of cyclopentanone aldol condensation MgO based catalysts by surface hydrophobization with organosilanes, *Appl. Catal. B-Environ.* 237 (2018) 835–843.
- [10] J. Fischer, W.F. Hölderich, Baeyer–Villiger-oxidation of cyclopentanone with aqueous hydrogen peroxide by acid heterogeneous catalysis, *Appl. Catal. A Gen.* 180 (1999) 435–443.
- [11] J. Yang, N. Li, G. Li, W. Wang, A. Wang, X. Wang, Y. Cong, T. Zhang, Synthesis of renewable high-density fuels using cyclopentanone derived from lignocellulose, *Chem. Commun.* 50 (2014) 2572–2574.
- [12] A.W. Beck, A.J. O'Brien, G.G. Zaites, D.E. Resasco, S.P. Crossley, V. Khanna, Systems-level analysis of energy and greenhouse gas emissions for coproducing biobased fuels and chemicals: implications for sustainability, *ACS Sustain. Chem. Eng.* (2018) 5826–5834.
- [13] S. Sittithisa, T. Pham, T. Prasomsri, T. Sooknoi, R.G. Mallinson, D.E. Resasco, Conversion of furfural and 2-methylpentanal on Pd/SiO<sub>2</sub> and Pd-Cu/SiO<sub>2</sub> catalysts, *J. Catal.* 280 (2011) 17–27.
- [14] S. Sittithisa, W. An, D.E. Resasco, Selective conversion of furfural to methylfuran over silica-supported Ni-Fe bimetallic catalysts, *J. Catal.* 284 (2011) 90–101.
- [15] T. Prasomsri, T. Nimmanwudipong, Y. Román-Leshkov, Effective hydrodeoxygenation of biomass-derived oxygenates into unsaturated hydrocarbons by MoO<sub>3</sub> using low H<sub>2</sub> pressures, *Energy Environ. Sci.* 6 (2013) 1732–1738.
- [16] Z. Zhao, R. Bababrik, W. Xue, Y. Li, N.M. Briggs, D.-T. Nguyen, U. Nguyen, S.P. Crossley, S. Wang, B. Wang, D.E. Resasco, Solvent-mediated charge separation drives alternative hydrogenation path of furanics in liquid water, *Nat. Catal.* 1 (2019), <https://doi.org/10.1038/s41929-019-0257-z>.
- [17] Y. Li, Z. Liu, Y. Liu, S.P. Crossley, F.C. Jentoft, S. Wang, Hydrogenation of o-cresol at



- the water/Pt (111) interface, *J. Phys. Chem. C* 123 (2019) 5378–5384.
- [18] J. Shangquan, Y.-H.C. Chin, Kinetic significance of proton–electron transfer during condensed phase reduction of carbonyls on transition metal clusters, *ACS Catal.* 9 (2019) 1763–1778.
  - [19] O.A. Abdelrahman, D.S. Park, K.P. Vinter, C.S. Spanjers, L. Ren, H.J. Cho, D.G. Vlachos, W. Fan, M. Tsapatsis, P.J. Dauenhauer, Biomass-derived butadiene by dehydro-decylization of tetrahydrofuran, *ACS Sustain. Chem. Eng.* 5 (2017) 3732–3736.
  - [20] ICIS Chemical Profile, Cyclopentadiene, (2007) <https://www.icis.com/resources/news/2007/07/16/9044783/chemical-profile-dicyclopentadiene/>.
  - [21] C. Piutti, F. Quartieri, The Piancatelli rearrangement: new applications for an intriguing reaction, *Molecules* 18 (2013) 12290–12312.
  - [22] M. Hronec, K. Fulajtarova, T. Liptaj, Effect of catalyst and solvent on the furan ring rearrangement to cyclopentanone, *Appl. Catal. A-Gen.* 437 (2012) 104–111.
  - [23] M. Hronec, K. Fulajtarova, T. Sotak, Highly selective rearrangement of furfuryl alcohol to cyclopentanone, *Appl. Catal. B-Environ.* 154 (2014) 294–300.
  - [24] M. Hronec, K. Fulajtarova, Selective transformation of furfural to cyclopentanone, *Catal. Commun.* 24 (2012) 100–104.
  - [25] Q. Zhang, J. Chang, T. Wang, Y. Xu, Review of biomass pyrolysis oil properties and upgrading research, *Energy Convers. Manage.* 48 (2007) 87–92.
  - [26] S. Czernik, A. Bridgwater, Overview of applications of biomass fast pyrolysis oil, *Energy Fuels* 18 (2004) 590–598.
  - [27] J. Meng, J. Park, D. Tilotta, S. Park, The effect of torrefaction on the chemistry of fast-pyrolysis bio-oil, *Bioresour. Technol.* 111 (2012) 439–446.
  - [28] T.R. Carlson, T.P. Vispute, G.W. Huber, Green gasoline by catalytic fast pyrolysis of solid biomass derived compounds, *ChemSusChem* 1 (2008) 397–400.
  - [29] L.A. Badovskaya, L.V. Povarova, Oxidation of furans (review), *Chem. Heterocycl. Compd.* 45 (2009) 1023–1034.
  - [30] N.A. Milas, W.L. Walsh, Catalytic oxidations. I. Oxidations in the furan series, *J. Am. Chem. Soc.* 57 (1935) 1389–1393.
  - [31] A. Takagaki, S. Nishimura, K. Ebitani, Catalytic transformations of biomass-derived materials into value-added chemicals, *Catal. Surv. From Asia* 16 (2012) 164–182.
  - [32] S. Wang, Y. Leng, F. Lin, C. Huang, C. Yi, Catalytic oxidation of furfural in vapor-gas phase for producing maleic anhydride, *Chem. Ind. Eng. Progress* 6 (2009) 029.
  - [33] E.R. Nielsen, Vapor phase oxidation of furfural, *Ind. Eng. Chem.* 41 (1949) 365–368.
  - [34] J. Kijenski, P. Winiarek, T. Paryczak, A. Lewicki, A. Mikolajska, Platinum deposited on monolayer supports in selective hydrogenation of furfural to furfuryl alcohol, *Appl. Catal. A-Gen.* 233 (2002) 171–182.
  - [35] H.Y. Zheng, Y.L. Zhu, B.T. Teng, Z.Q. Bai, C.H. Zhang, H.W. Xiang, Y.W. Li, Towards understanding the reaction pathway in vapour phase hydrogenation of furfural to 2-methylfuran, *J. Mol. Catal. A-Chem.* 246 (2006) 18–23.
  - [36] Y.L. Zhu, H.W. Xiang, Y.W. Li, H.J. Jiao, G.S. Wu, B. Zhong, G.Q. Guo, A new strategy for the efficient synthesis of 2-methylfuran and gamma-butyrolactone, *New J. Chem.* 27 (2003) 208–210.
  - [37] J. Yang, H.Y. Zheng, Y.L. Zhu, G.W. Zhao, C.H. Zhang, B.T. Teng, H.W. Xiang, Y.W. Li, Effects of calcination temperature on performance of Cu-Zn-Al catalyst for synthesizing gamma-butyrolactone and 2-methylfuran through the coupling of dehydrogenation and hydrogenation, *Catal. Commun.* 5 (2004) 505–510.
  - [38] H.Y. Zheng, J. Yang, Y.L. Zhu, G.W. Zhao, Synthesis of gamma-butyrolactone and 2-methylfuran through the coupling of dehydrogenation and hydrogenation over copper-chromite catalyst, *React. Kinet. Catal. Lett.* 82 (2004) 263–269.
  - [39] T. Omotoso, S. Boonyasuwat, S.P. Crossley, Understanding the role of TiO<sub>2</sub> crystal structure on the enhanced activity and stability of Ru/TiO<sub>2</sub> catalysts for the conversion of lignin-derived oxygenates, *Green Chem.* 16 (2014) 645–652.
  - [40] N.M. Briggs, L. Barrett, E.C. Wegener, L.V. Herrera, L.A. Gomez, J.T. Miller, S.P. Crossley, Identification of active sites on supported metal catalysts with carbon nanotube hydrogen highways, *Nat. Commun.* 9 (2018) 3827.
  - [41] G. Kresse, J. Furthmüller, Efficient iterative schemes for ab initio total-energy calculations using a plane-wave basis set, *Phys. Rev. B* 54 (1996) 11169–11186.
  - [42] J.P. Perdew, K. Burke, M. Ernzerhof, Generalized gradient approximation made simple, *Phys. Rev. Lett.* 77 (1996) 3865–3868.
  - [43] P.E. Blochl, Projector augmented-wave method, *Phys. Rev. B* 50 (1994) 17953–17979.
  - [44] G. Kresse, D. Joubert, From ultrasoft pseudopotentials to the projector augmented-wave method, *Phys. Rev. B* 59 (1999) 1758–1775.
  - [45] S. Grimme, J. Antony, S. Ehrlich, H. Krieg, A consistent and accurate ab initio parametrization of density functional dispersion correction (DFT-D) for the 94 elements H–Pu, *J. Chem. Phys.* 132 (2010) 154104.
  - [46] S. Grimme, S. Ehrlich, L. Goerigk, Effect of the damping function in dispersion corrected density functional theory, *J. Comput. Chem.* 32 (2011) 1456–1465.
  - [47] A.I. Liechtenstein, V.I. Anisimov, J. Zaanen, Density-functional theory and strong-interactions – orbital ordering in mott-hubbard insulators, *Phys. Rev. B* 52 (1995) R5467–R5470.
  - [48] Z.P. Hu, H. Metiu, Choice of U for DFT plus U calculations for titanium oxides, *J. Phys. Chem. C* 115 (2011) 5841–5845.
  - [49] B. Wang, M.L. Bocquet, S. Marchini, S. Gunther, J. Wintterlin, Chemical origin of a graphene moire overlayer on Ru(0001), *Phys. Chem. Chem. Phys.* 10 (2008) 3530–3534.
  - [50] J. Zhang, B. Wang, E. Nikolla, J.W. Medlin, Directing reaction pathways through controlled reactant binding at Pd-TiO<sub>2</sub> interfaces, *Angew. Chem. Int. Ed.* 56 (2017) 6594–6598.
  - [51] D. Scholz, C. Aellig, I. Hermans, Catalytic transfer hydrogenation/hydrogenolysis for reductive upgrading of furfural and 5-(hydroxymethyl)furfural, *ChemSusChem* 7 (2014) 268–275.
  - [52] S. Sithisa, T. Sooknoi, Y.G. Ma, P.B. Balbuena, D.E. Resasco, Kinetics and mechanism of hydrogenation of furfural on Cu/SiO<sub>2</sub> catalysts, *J. Catal.* 277 (2011) 1–13.
  - [53] S. Sithisa, D.E. Resasco, Hydrodeoxygenation of furfural over supported metal catalysts: a comparative study of Cu, Pd and Ni, *Catal. Lett.* 141 (2011) 784–791.
  - [54] T. Komaya, A.T. Bell, Z. Wengsieh, R. Gronsky, F. Engelke, T.S. King, M. Pruski, Effects of dispersion and metal-metal oxide interactions on Fischer-Tropsch synthesis over Ru/TiO<sub>2</sub> and TiO<sub>2</sub>-promoted Ru/SiO<sub>2</sub>, *J. Catal.* 150 (1994) 400–406.
  - [55] R.C. Nelson, B. Baek, P. Ruiz, B. Goundie, A. Brooks, M.C. Wheeler, B.G. Frederick, L.C. Grabow, R.N. Austin, Experimental and Theoretical Insights into the Hydrogen-Efficient Direct Hydrodeoxygenation Mechanism of Phenol over Ru/TiO<sub>2</sub>, *ACS Catal.* 5 (2011) 6509–6523.
  - [56] D.E. Resasco, G.L. Haller, A model of metal-oxide support interaction for Rh on TiO<sub>2</sub>, *J. Catal.* 82 (1983) 279–288.
  - [57] N.R. Avery, Eels identification of the adsorbed species from acetone adsorption on Pt(111), *Surf. Sci.* 125 (1983) 771–786.
  - [58] R. Shekhar, M.A. Barteau, R.V. Plank, J.M. Vohs, Adsorption and reaction of aldehydes on Pd surfaces, *J. Phys. Chem. B* 101 (1997) 7939–7951.
  - [59] J.L. Davis, M.A. Barteau, Polymerization and decarbonylation reactions of aldehydes on the Pd(111) surface, *J. Am. Chem. Soc.* 111 (1989) 1782–1792.
  - [60] M. Hronec, K. Fulajtarová, I. Vávra, T. Soták, E. Dobročka, M. Mičušfík, Carbon supported Pd–Cu catalysts for highly selective rearrangement of furfural to cyclopentanone, *Appl. Catal. B* 181 (2016) 210–219.
  - [61] S. Boonyasuwat, T. Omotoso, D.E. Resasco, S.P. Crossley, Conversion of guaiacol over supported Ru catalysts, *Catal. Lett.* 143 (2013) 783–791.
  - [62] T.O. Omotoso, B. Baek, L.C. Grabow, S.P. Crossley, Experimental and first-principles evidence for interfacial activity of Ru/TiO<sub>2</sub> for the direct conversion of m-cresol to toluene, *ChemCatChem* 9 (2017) 2642–2651.
  - [63] V. Selvaraj, M. Vinoba, M. Alagar, Electrocatalytic oxidation of ethylene glycol on Pt and Pt-Ru nanoparticles modified multi-walled carbon nanotubes, *J. Colloid Interface Sci.* 322 (2008) 537–544.
  - [64] T. Iwasita, Electrocatalysis of methanol oxidation, *Electrochim. Acta* 47 (2002) 3663–3674.
  - [65] J. Jiang, A. Kucernak, Electrooxidation of small organic molecules on mesoporous precious metal catalysts, *J. Electroanal. Chem.* 543 (2003) 187–199.
  - [66] Q. Tan, G. Wang, L. Nie, A. Dinse, C. Buda, J. Shabaker, D.E. Resasco, Different product distributions and mechanistic aspects of the hydrodeoxygenation of m-cresol over platinum and ruthenium catalysts, *ACS Catal.* 5 (2015) 6271–6283.
  - [67] J.E. Rekoske, M.A. Barteau, Isothermal reduction kinetics of titanium dioxide-based materials, *J. Phys. Chem. B* 101 (1997) 1113–1124.
  - [68] T.N. Pham, T. Sooknoi, S.P. Crossley, D.E. Resasco, Ketoneization of carboxylic acids: mechanisms, catalysts, and implications for biomass conversion, *ACS Catal.* 3 (2013) 2456–2473.
  - [69] D.E. Resasco, S.P. Crossley, Implementation of concepts derived from model compound studies in the separation and conversion of bio-oil to fuel, *Catal. Today* 257 (2015) 185–199.
  - [70] J.A. Herron, T. Vann, N. Duong, D.E. Resasco, S. Crossley, L.L. Lobban, C.T. Maravelias, A systems-level roadmap for biomass thermal fractionation and catalytic upgrading strategies, *Energy Technol.* 5 (2017) 130–150.
  - [71] G.G. Zaimes, A.W. Beck, R.R. Janupala, D. Resasco, S. Crossley, L.L. Lobban, V. Khanna, Multistage torrefaction and in situ catalytic upgrading to hydrocarbon biofuels: analysis of life cycle energy use and greenhouse gas emissions, *Energy Environ. Sci.* 10 (2017) 1034–1050.

## Further reading

- P.S. Deimel, R.M. Bababrik, B. Wang, P.J. Blowey, L.A. Rochford, P.K. Thakur, T.-L. Lee, M.-L. Bocquet, J.V. Barth, D.P. Woodruff, D.A. Duncan, F.A. Allegretti, Direct quantitative identification of the “surface trans-effect”, *Chem. Sci.* 7 (2016) 5647–5656.